A&A 382, 688–698 (2002)
DOI: 10.1051/0004-6361:20011599

Astronomy & Astrophysics

Diagnostics of electron bombardment in solar flares from hydrogen Balmer lines

J. Kašparová⋆ and P. Heinzel

Astronomical Institute, Academy of Sciences of the Czech Republic, Fričova 298, Ondřejov, 25165, The Czech Republic

Received 23 July 2001 / Accepted 8 November 2001

Abstract. Influence of non-thermal collisional rates, related to an electron beam, on hydrogen Balmer line profiles is investigated. Semi-empirical temperature structure of the flare model F1 has been used for computing non-LTE profiles of Hα, Hβ, and Hγ. Contribution functions and their change due to different values of beam parameters are shown. Unlike the line core intensity, the intensity of line wings considerably depends on beam parameters and it is significantly enhanced for typical values of the beam energy flux. The ratio of line intensities at a selected wavelength is proposed to be used for diagnostics of electron beams during solar flares, particularly at impulsive phases. Obtained Hα line profiles are compared to those of Fang et al. (1993).

Key words. Sun: flares – line: profiles – methods: numerical

1. Introduction

Solar flare energy is believed to be released in the low corona and then transported downwards into lower dense chromospheric layers by various mechanisms. One of them is an electron beam bombardment. Hard X-ray observations indicate that electron beams lose their energy in collisions with ambient plasma. Therefore, a study of chromospheric response to pulse beam heating is important. In order to investigate the influence of accelerated particle beams on spectral line profiles, non-thermal collisional rates have to be considered. Non-thermal collisional ionisation of hydrogen was first taken into account by Hudson (1971); Brown (1972); Lin & Hudson (1976). First expressions of non-thermal collisional excitation rates were given by Chambe & Hénoux (1979).

Most of computations of spectral line profiles have been done for static flare models. One approach in theoretical static flare modelling is to specify mechanisms of a flare heating. In such models the energy equation is solved simultaneously with the equations describing the pressure balance, the radiative transfer, and the statistical equilibrium. Study of the effects of various heating mechanisms on Hα line profiles was done by Canfield et al. (1984) and Hawley & Fisher (1994). Non-thermal electron collisional rates and heating by non-thermal electrons were treated in Canfield et al. (1984), which is based on energy-balance models of Ricchiazzi & Canfield (1983). A set of one dimensional, static models of flare atmospheres was developed, each model was determined by four independent parameters describing the flare corona: P_0 (the coronal pressure), F_5 (conductive flux at $T = 10^5$ K) and the non-thermal electron flux above 20 keV F_{20}. Hα line profiles were calculated by solving the probabilistic radiative transfer equation for a four-level plus continuum hydrogen atomic model.

In their 1D static models, Hawley & Fisher (1994) assumed an X-ray heating of the chromosphere and heating by non-thermal electrons. The non-thermal collisional ionisation rates were also included into the statistical equilibrium equations; the radiation transport equations were used for obtaining Hα line profiles. The models were divided into three types: impulsive (density distribution frozen in the pre-flare state), evolving (hydrostatic equilibrium holds but energetic equilibrium has not been established in the corona), and equilibrium (the whole atmosphere in hydrostatic and energetic equilibrium). It was concluded that observed Hα profiles could be reproduced by the impulsive models of low coronal pressure with strong non-thermal heating.

Finally, Fang et al. (1993) included the non-thermal collisional excitation and ionisation rates due to electron beams into semi-empirical models. Their computations are based on the temperature distributions given by flare models F1 and F2 of Machado et al. (1980). These well-known semi-empirical models are based on spectral observations

Send offprint requests to: J. Kašparová,
e-mail: kasparov@asu.cas.cz

⋆ This work was done as a part of Ph.D. study at the Faculty of Mathematics and Physics of Charles University, Prague.

of several flares obtained during various phases of their evolution (note that some of these flares were observed after their maximum and thus F1 or even F2 can be used as well for the gradual phase). The presence of beams during the impulsive phase has two effects: (i) heating due to energy dissipation and (ii) non-thermal excitation and ionisation of various species. The heating is implicitly included into the semi-empirical temperature structure which Fang et al. (1993) assumed to be fixed. Then they studied so called *differential* effect of non-thermal collisional rates on spectral line intensities, i.e. they compared the line profiles in presence and without presence of beams for the same atmospheric model. In their models the statistical equilibrium equations and the radiative transfer equations, together with the equation of hydrostatic equilibrium, were solved iteratively. Hα and CaII line profiles were calculated by using a four-level plus continuum atomic model of hydrogen and a five-level plus continuum atomic model of ionised calcium, respectively. Hα line profiles obtained for chosen beam parameters show a substantial increase in line intensities by a factor up to 5. Namely the line core intensities vary significantly with beam parameters. Recently, the optical effects of the non-thermal particle bombardment of the solar atmosphere have been reviewed by Fang et al. (2000), Hénoux (2000).

In the present paper we follow the approach of Fang et al. (1993) in order to demonstrate the differential effects of the non-thermal collisional rates on other Balmer lines (Hβ, Hγ). We analyse the contribution functions of Balmer lines and study their depth variations due to beam energy deposit on hydrogen for different parameters of the electron beam.

The paper has been organised in the following manner: Sect. 2 presents relations between the non-thermal collisional rates and characteristics of the electron beam; values of beam parameters are set there. Brief description of numerical models is given in Sect. 3. Effects of the non-thermal collisional rates are discussed in Sect. 4 by showing computed line profiles and contribution functions of Hα, Hβ, and Hγ. Intensity ratio method as a possible diagnostic tool is proposed there. In Sect. 5 we compare our results for Hα with the work of Fang et al. (1993). Section 6 summarises our results.

2. Rate of energy deposit and non-thermal collisional rates

Beam particles lose their energy in collisions with ambient neutral and charged targets. Here we will concentrate only on the electron bombardment. Under assumption that the energy is deposited in the atmosphere mainly due to collisions with electrons, protons, and hydrogen atoms, the rate of energy deposit on hydrogen $\mathrm{d}E_\mathrm{H}/\mathrm{d}t$ at a column density N follows from Emslie (1978), Chambe & Hénoux (1979), Emslie (1981), Ricchiazzi (1982), Hawley & Fisher (1994):

$$\frac{\mathrm{d}E_\mathrm{H}}{\mathrm{d}t} = \frac{Kn}{2\mu_0}(1-x)\Lambda'(\delta-2)B_{x_1}\left(\frac{\delta}{2},\frac{2}{4+\beta}\right)\frac{\mathcal{F}_1}{E_1^2}\left(\frac{N}{N_1}\right)^{-\frac{\delta}{2}}. \quad (1)$$

Electron energy flux with a power index δ is

$$F(E_0) = (\delta-2)\,\frac{\mathcal{F}_1}{E_1^2}\left(\frac{E_0}{E_1}\right)^{-\delta}, \quad (2)$$

where $\mathcal{F}_1$ equals to the total electron energy flux above the cutoff energy E_1. B_{x_1} is the incomplete beta function with $x_1 = N/N_1$ for $x_1 < 1$, otherwise $x_1 = 1$. N_1 corresponds to the deepest column density reached by electrons with initial energy E_1; n represents the hydrogen number density, x is the ionised fraction of hydrogen, $K = 2\pi e^4$, μ_0 is the initial pitch angle of the beam. Parameter β is defined (Emslie 1981) by

$$\beta = \frac{2x\Lambda + (1-x)\Lambda''}{\Lambda' + x(\Lambda-\Lambda')}. \quad (3)$$

Λ is the Coulomb logarithm, Λ' and Λ'' are collisional logarithms related to inelastic and elastic electron collisions with neutrals. For their definitions see Emslie (1978).

The collisional logarithms Λ, Λ', and Λ'' are depth dependent and can be expressed as functions of n and the beam electron energy E (ergs) (Ricchiazzi 1982): $\Lambda = 1.5\ \ln(E) - 0.5\ln(n) + 65.1$, $\Lambda' = \ln(E) + 25.1$, and $\Lambda'' = 0.5\ln(E) + 12.3$. We follow the approach of Hawley & Fisher (1994) and treat their values as constants for the whole atmosphere. Assuming $E_1 = 20$ keV and $\mu_0 = 1$, mean values of the collisional logarithms have been computed by using average injected beam electron energies ($\delta = 3$, 4, and 5). $\Lambda = 25$, $\Lambda' = 8$, and $\Lambda'' = 4$.

The expression for the rate of the energy deposit (1) was derived by keeping the parameter β (Eq. (3)) constant along the path of a beam electron. However, Eq. (1) varies only slightly with β. Assuming a value of the mean ionised fraction of hydrogen $\bar{x} = 0.5$ (middle chromosphere), we have set $\beta = 2$ and similarly $\gamma = 17$.

There is a direct connection between the rate of energy deposit on hydrogen $\mathrm{d}E_\mathrm{H}/\mathrm{d}t$ and the non-thermal collisional excitation C_{1i}^nt and ionisation $C_{1\mathrm{c}}^\mathrm{nt}$ rates of hydrogen. We have adopted the same approach as Fang et al. (1993):

$$\begin{aligned}
C_{1\mathrm{c}}^\mathrm{nt} &= 1.73\times10^{10}\frac{1}{n_1}\frac{\mathrm{d}E_\mathrm{H}}{\mathrm{d}t}\\
C_{12}^\mathrm{nt} &= 2.94\times10^{10}\frac{1}{n_1}\frac{\mathrm{d}E_\mathrm{H}}{\mathrm{d}t}\\
C_{13}^\mathrm{nt} &= 5.35\times10^{9}\frac{1}{n_1}\frac{\mathrm{d}E_\mathrm{H}}{\mathrm{d}t}\\
C_{14}^\mathrm{nt} &= 1.91\times10^{9}\frac{1}{n_1}\frac{\mathrm{d}E_\mathrm{H}}{\mathrm{d}t}.
\end{aligned} \quad (4)$$

For further details see Fang's paper. The collisional deexcitations by non-thermal electrons have been neglected (Feautrier & Sahal-Bréchot, private communication). We consider only classical collisional deexcitations by thermal electrons.

3. Numerical approach to non-LTE models of flares

We have solved the non-LTE radiative-transfer problem using the semi-empirical flare-atmosphere model F1 (Machado et al. 1980), with a given temperature distribution. Our code uses a static, 1D plane-parallel geometry and the atmosphere is in hydrostatic equilibrium as in Machado et al. (1980). We thus neglect the macroscopic velocity fields because our primary objective is to study the differential effects of non-thermal collisions on spectral-line profiles. Hydrogen excitation and ionisation equilibrium has been computed by solving simultaneously the radiative transfer equations, the equations of statistical equilibrium and the equation of particle and charge conservation. The equations of statistical equilibrium have been preconditioned according to Rybicki & Hummer (1991). The preconditioning is based on the Lambda-operator splitting technique, where the exact Lambda-operator is expressed as an approximate operator plus the correction. Then the correction is computed iteratively by so-called Accelerated Lambda Iteration (ALI) method which is much faster and reliable as compared to standard Lambda iterations (see discussion below). The preconditioned equations are then linearised with respect to particle densities and atomic level populations (Heinzel 1995) and solved iteratively. This method is referred to as the MALI (Multilevel Accelerated Lambda Iterations) method. The non-thermal collisional excitation and ionisation rates evaluated for different values of electron beam parameters δ and $\mathcal{F}_1$ have been included into the statistical equilibrium equations using the expressions in Eq. (4). MALI has been used to solve the transfer problem for a five-level plus continuum atomic model of hydrogen. Number of non-thermal collisional transitions is equal to $n_1 C_{1j}^{\rm nt}$, where the non-thermal collisional rates were calculated by using the value of hydrogen number density in the ground level from the previous iteration (see Eq. (4)). Finally we have computed the normally emergent profiles of three Balmer lines, where we have taken into account the microturbulent and Stark broadening effects.

4. Effects of non-thermal collisional rates

4.1. Line profiles

Profiles of three Balmer lines Hα, Hβ, and Hγ computed for different values of δ and $\mathcal{F}_1$ by using the model F1 are plotted in Figs. 1–3. Corresponding line profiles without including the non-thermal collisional rates (dotted line) are also displayed in each figure. All figures show that the line-wing intensities significantly rise with increasing the total electron energy flux $\mathcal{F}_1$, while the effects in line cores are only marginal. In contrast, the line intensities are much less sensitive to different values of the parameter δ. The line core intensity is increased in comparison with the line intensity of profile without including non-thermal collisional rates. However, there is only weak dependence of the line core intensity on values of δ or $\mathcal{F}_1$. This latter result contrasts with that of Fang et al. (1993) (see discussion below).

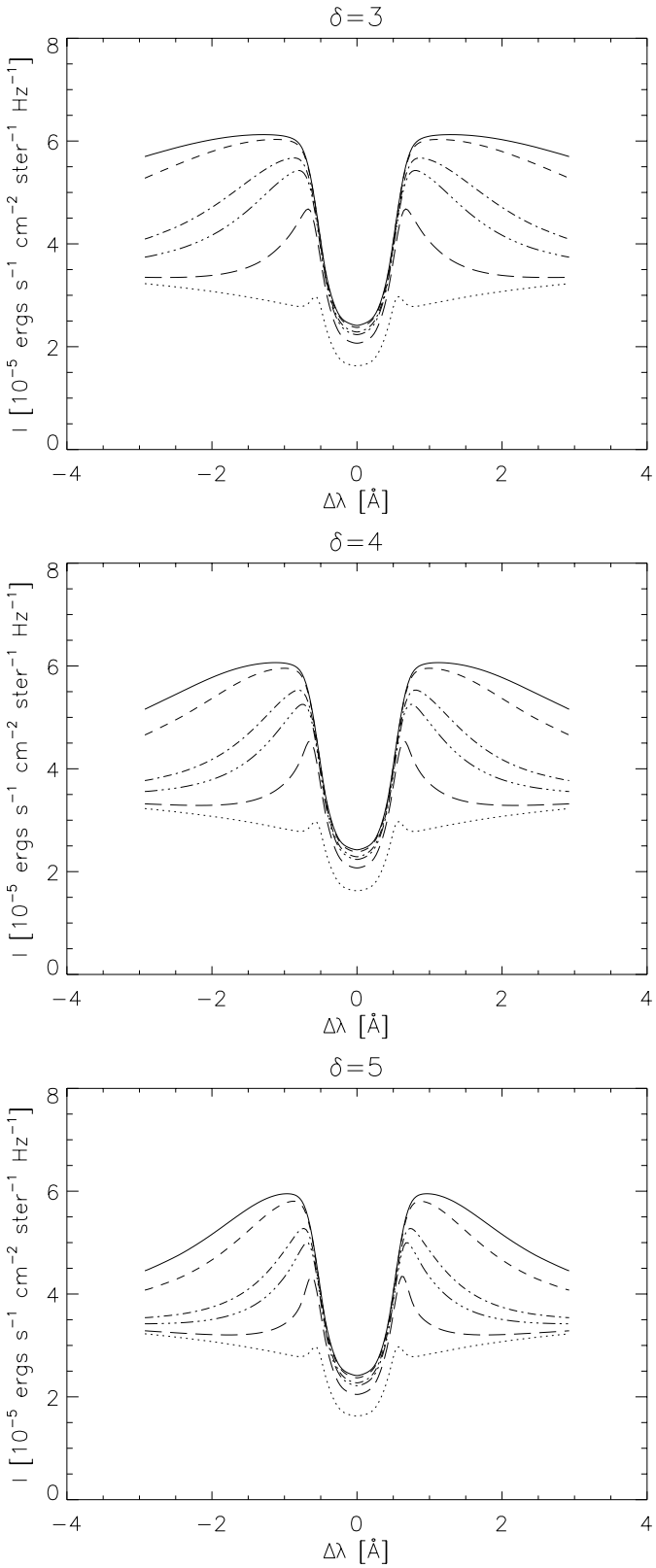

Fig. 1. Hα line profiles for δ = 3, 4, 5 and $\mathcal{F}_1 = 10^{12}$ (solid), 5×10^{11} (dashed), 10^{11} (dash dot), 5×10^{10} (dash dot dot dot), and 10^{10} (long dash) ergs cm^{-2} s^{-1}. Dotted lines indicate profiles without including the non-thermal collisional rates.

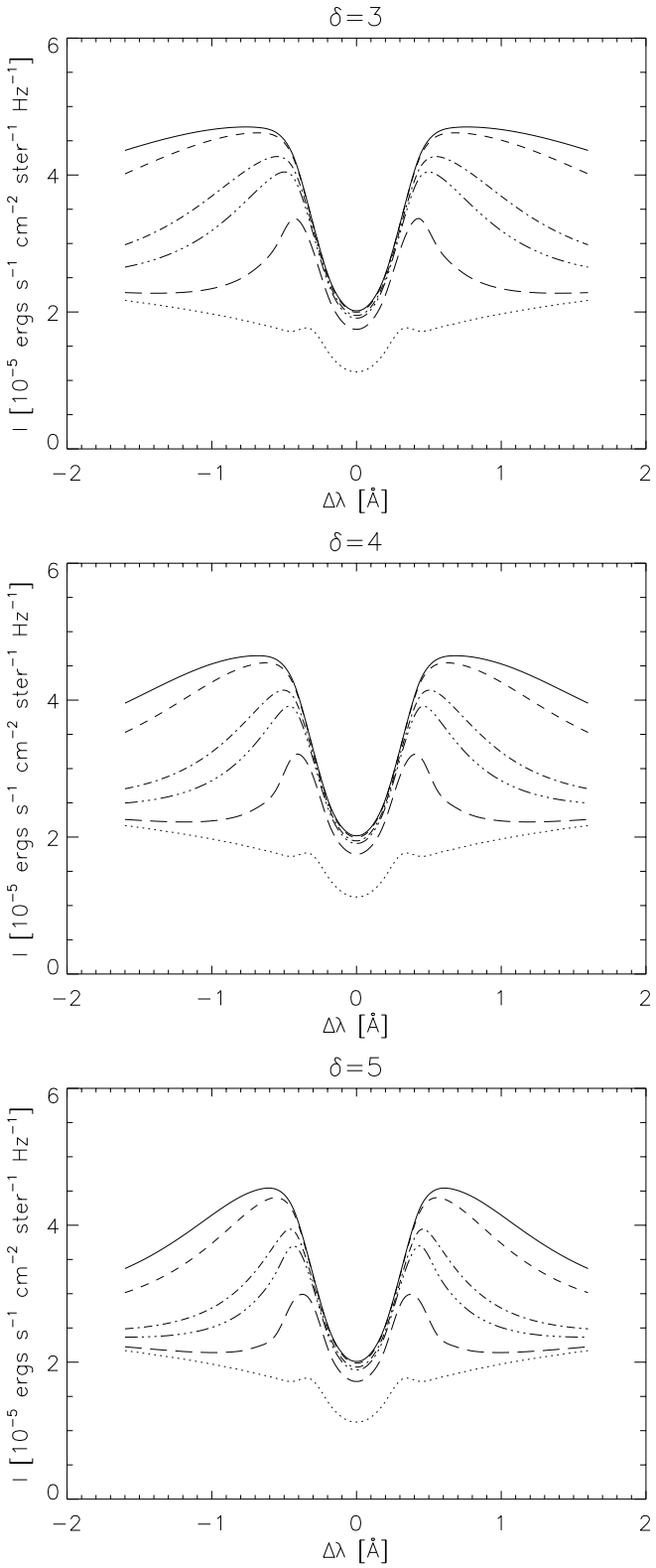

Fig. 2. Hβ line profiles for δ = 3, 4, 5 and $\mathcal{F}_1 = 10^{12}$ (solid), 5×10^{11} (dashed), 10^{11} (dash dot), 5×10^{10} (dash dot dot dot), and 10^{10} (long dash) ergs cm^{-2} s^{-1}. Dotted lines indicate profiles without including the non-thermal collisional rates.

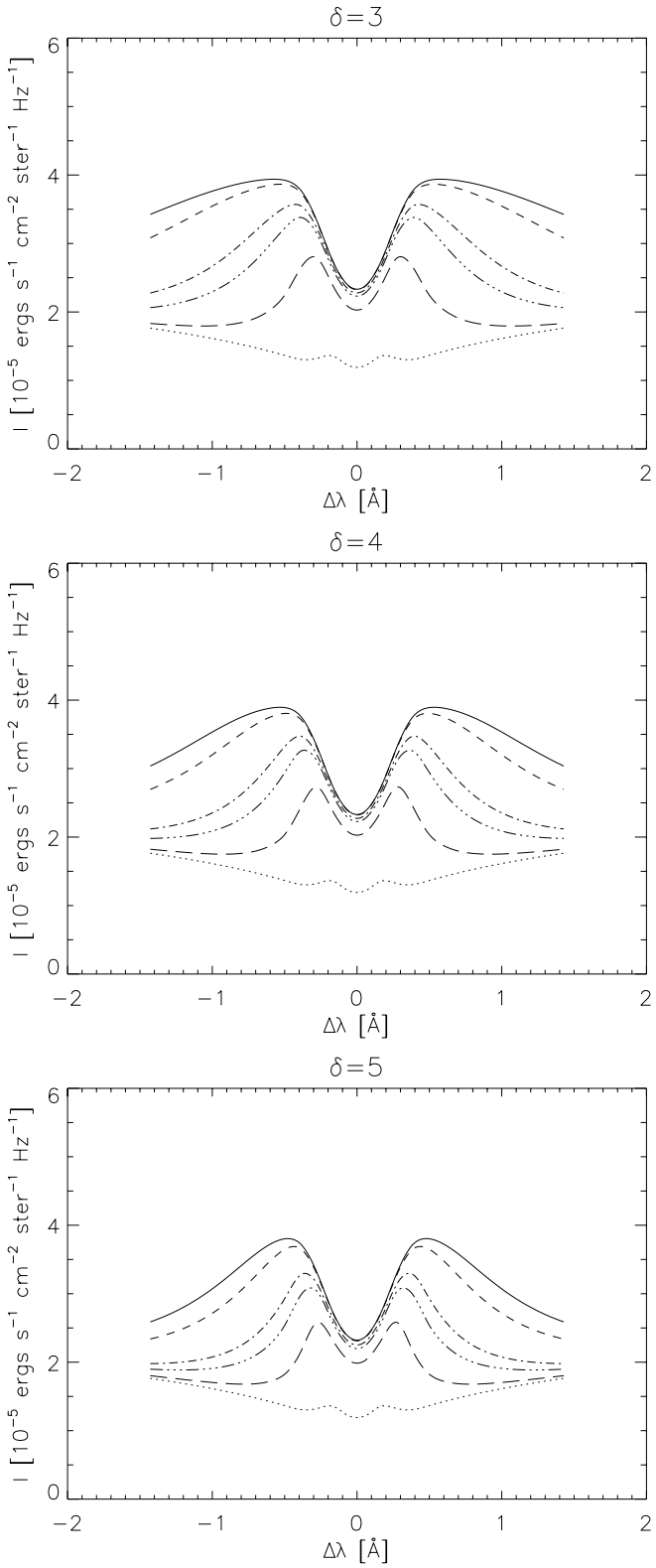

Fig. 3. Hγ line profiles for δ = 3, 4, 5 and $\mathcal{F}_1 = 10^{12}$ (solid), 5×10^{11} (dashed), 10^{11} (dash dot), 5×10^{10} (dash dot dot dot), and 10^{10} (long dash) ergs cm^{-2} s^{-1}. Dotted lines indicate profiles without including the non-thermal collisional rates.

4.2. Contribution functions

The effect of different values of $\mathcal{F}_1$ is considerably pronounced in the line wings. This behaviour is closely associated with a formation depth of the line intensity in specific wavelengths. Figures 9–11 display the contribution

functions CF as a 2D function of the line centre wavelength and the depth h. By definition

$$I_\nu(0) = \int CF \, \mathrm{d}h, \tag{5}$$

where $I_\nu(0)$ is the emergent specific intensity. For semi-infinite atmosphere a formal solution of the equation of radiative transfer has the form (for normally outgoing radiation)

$$I_\nu(0) = \int_0^\infty S_\nu(t_\nu) \, \mathrm{e}^{-t_\nu} \, \mathrm{d}t_\nu. \tag{6}$$

Using $\mathrm{d}t_\nu = -\chi_\nu \, \mathrm{d}h$ and $S_\nu = \eta_\nu/\chi_\nu$, we obtain

$$CF = \eta_\nu(h) \, \mathrm{e}^{-t_\nu(h)}. \tag{7}$$

S_ν is the line source function, η_ν is the emission coefficient, χ_ν is the absorption coefficient, and t_ν is the optical depth.

On each of Figs. 9–11 the first image refers to the contribution function of Hα, Hβ, or Hγ without including the non-thermal collisional rates. The corresponding rate of the energy deposit on hydrogen is over-plotted on subsequent four images. These figures clearly show that formation of the line wing intensities moves to higher parts of the atmosphere as the value of $\mathcal{F}_1$ rises, whereas the location of formation region of the line core intensities remains approximately the same.

Most of the contribution functions exhibit a gap of low values which separates the regions where significant portions of the line intensity are formed. The gap is caused by a drop of the second level and high-level populations of hydrogen near the temperature minimum. The drop in the second level population results in more transparent medium in the region of the gap and thus we see contributions from the photospheric layers. Values of η_ν in the temperature minimum are also lower because of the drop of high-level populations. Combination of these effects leads to a decrease in the contribution functions.

Keeping $\mathcal{F}_1$ constant, maximum of the rate of energy deposit on hydrogen reaches deeper layers of atmosphere for $\delta = 3$ than for the case of $\delta = 5$. This behaviour is mainly a result of the form of Eq. (2) and the condition for the maximum of $\mathrm{d}E_\mathrm{H}/\mathrm{d}t$:

$$\frac{\mathrm{d}\ln n(1-x)}{\mathrm{d}h} = \frac{\delta}{2}\frac{\mathrm{d}\ln N}{\mathrm{d}h} \tag{8}$$

($x_1 = 1$ for all N in atmosphere model F1). Lower values of δ imply more electrons with energy $E_0 > E_1$ which lose their energy in deeper parts of atmosphere. The maximum of the rate of energy deposit on hydrogen can also be shifted in depth only by changing the value of $\mathcal{F}_1$ (constant δ); see e.g. Fig. 9. The shift is given by different depth dependence of $(N/N_1)^{-\delta/2}$ corresponding to different values of $\mathcal{F}_1$. For discussion on the depth scale see Sect. 6.

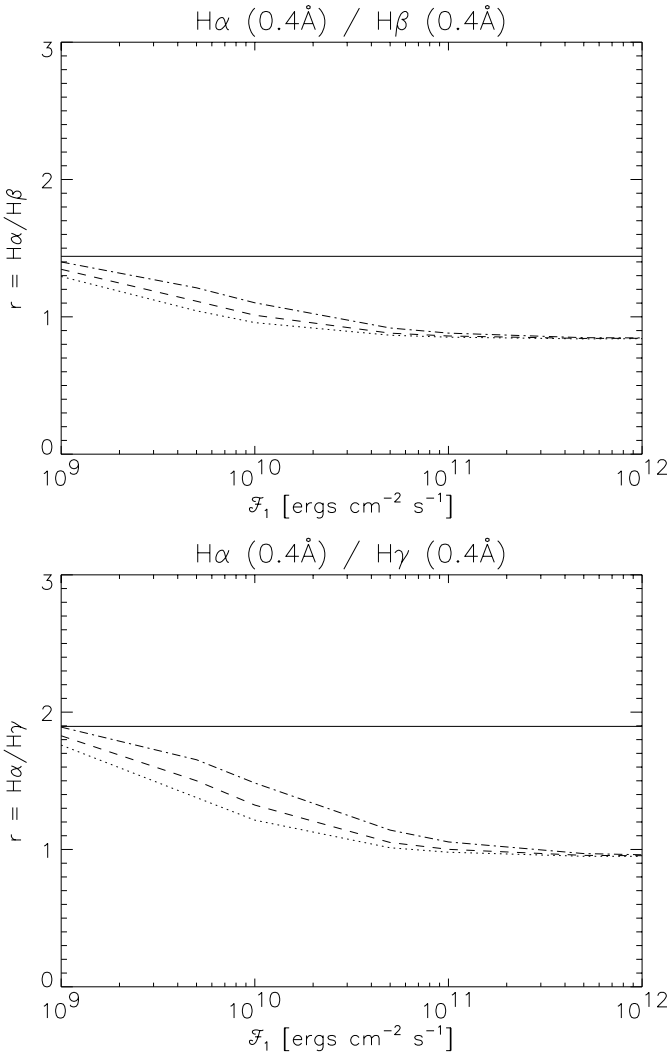

Fig. 4. Intensity ratio of Hα/Hβ, resp. Hα/Hγ versus the total electron energy flux $\mathcal{F}_1$ for $\delta = 3$ (dotted), 4 (dashed), and 5 (dash dot). Solid line indicates corresponding ratio without including the non-thermal collisional rates ($\mathcal{F}_1 = 0$).

4.3. Intensity ratios

Concerning diagnostic tools suitable for comparison of our theoretical line profiles with the observed ones, we suggest to use the intensity ratios. Figure 4 shows the ratio of Hα/Hβ, resp. Hα/Hγ intensities as a function of the total energy flux $\mathcal{F}_1$ at a selected wavelength. In order to get a unique solution for $\mathcal{F}_1$ using the intensity ratios, we require a monotonic dependence of the ratios on $\mathcal{F}_1$. However, the monotonic dependence seems to be a rather strong condition since only few combinations of $\Delta\lambda$ satisfy it. We have selected $\Delta\lambda = 0.4$ Å for all considered lines which reveals the most pronounced change of the intensity ratios over $\mathcal{F}_1$ values. The intensity ratios without including the non-thermal collisional rates are indicated by full line. The ratio of Hα/Hγ for $\mathcal{F}_1 = 10^{12}$ ergs cm^{-2} s^{-1} decreases nearly by 50% compared with the case without including the non-thermal collisional rates. Ratio Hα/Hβ

is lowered by 40%. The intensity ratios are little sensitive to different values of the power index δ.

The contribution functions at $\Delta\lambda = 0.4$ Å together with the rate of energy deposit are plotted in Fig. 5. These graphs show that the place from which the intensity $I_{\mathrm{H}\alpha}(\Delta\lambda = 0.4)$ originates varies only slightly with $\mathcal{F}_1$ in contrast with $I_{\mathrm{H}\beta}(\Delta\lambda = 0.4)$ or $I_{\mathrm{H}\gamma}(\Delta\lambda = 0.4)$. Although the contribution functions of Hβ, resp. Hγ, at $\Delta\lambda = 0.4$ are almost by a order of magnitude lower than for Hα, the resultant line intensities are comparable. This is caused by a different width of the region which significantly contributes to the line intensity (see Eq. (5)).

The intensity ratios start to saturate for $\mathcal{F}_1 > \mathcal{F}_1^{\mathrm{s}} = 10^{11}$ ergs cm^{-2} s^{-1}. We have found out that in region where hydrogen ionisation degree $x \geq 0.9$ populations of high levels are only slightly sensitive to the values of $\mathcal{F}_1$. $I_{\mathrm{H}\alpha}(\Delta\lambda = 0.4)$ comes from such part of atmosphere. Hence, χ_ν, η_ν, and $I_{\mathrm{H}\alpha}(\Delta\lambda = 0.4)$ do not considerably vary with $\mathcal{F}_1$ (see Fig. 1). However, $I_{\mathrm{H}\beta}(\Delta\lambda = 0.4)$ and $I_{\mathrm{H}\gamma}(\Delta\lambda = 0.4)$ contain contributions from deeper atmospheric layers in the case of $\mathcal{F}_1 < \mathcal{F}_1^{\mathrm{s}}$. As value of $\mathcal{F}_1$ is increased, second level population and thus χ_ν grow in these deeper layers due to higher values of non-thermal collisional rates. Consequently, contribution functions of Hβ and Hγ at $\Delta\lambda = 0.4$ Å show significant values only at the higher atmospheric layers (see Fig. 5), which are almost fully ionised. Therefore, resultant line intensities at $\Delta\lambda = 0.4$ Å are not sensitive to further increase of $\mathcal{F}_1$. This saturation effect is not a general behaviour but strongly depends on selected $\Delta\lambda$.

It must be pointed out that presented dependences of the intensity ratios on $\mathcal{F}_1$ reveal the effects of the non-thermal collisional rates for the case of the fixed temperature structure of the model F1. However, distinct temperature distribution may considerably influence the line intensities. Therefore, the intensity ratios will be model dependent.

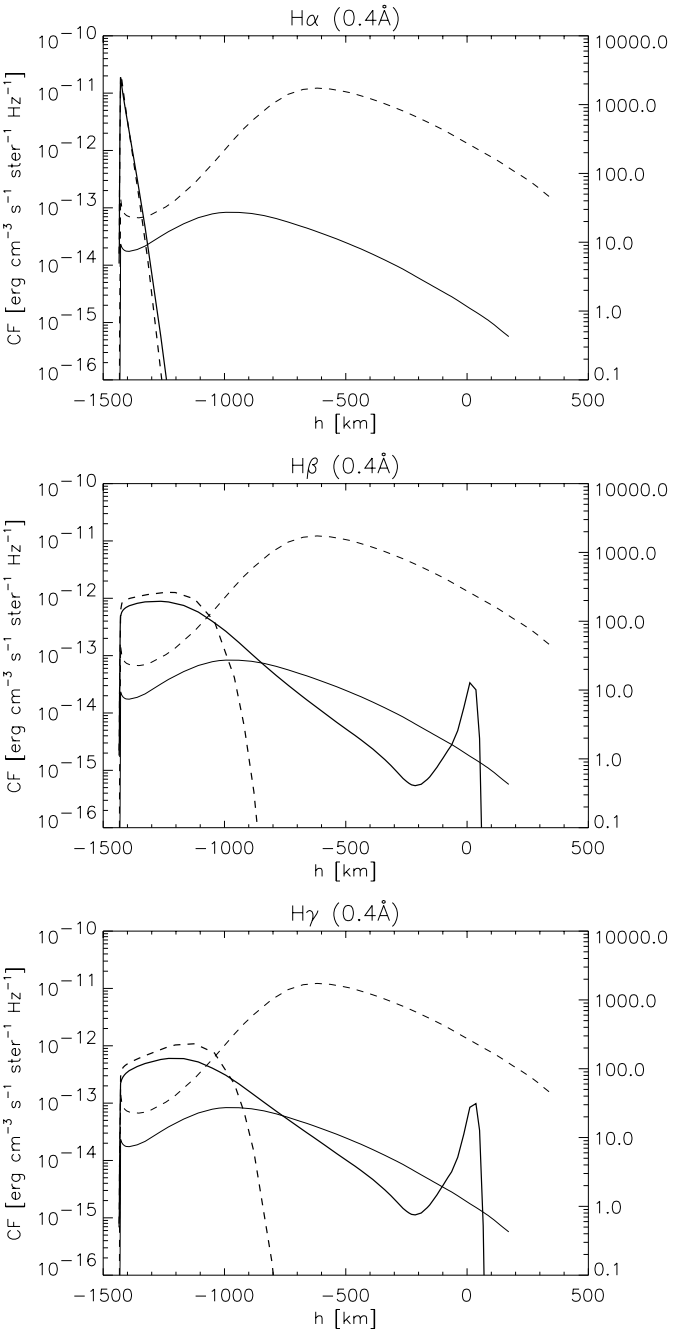

Fig. 5. Dependence of the contribution function CF at $\Delta\lambda = 0.4$ Å and the energy deposit rate on hydrogen $\mathrm{d}E_{\mathrm{H}}/\mathrm{d}t$ (thinner lines) on the height h for $\delta = 3$ and $\mathcal{F}_1 = 10^{10}$ (solid), and 10^{12} (dashed) ergs cm^{-2} s^{-1}.

5. Computational methods

At the beginning of our work we adopted the same approach as Fang et al. (1993) and expected to obtain very similar Hα line profiles. However, even though our column mass dependence of the collisional ionisation rates and electron density give almost the same results as those presented in Hénoux et al. (1993, Fig. 5), or Fang et al. (1993, Fig. 4), our Hα line profiles do not show as strong intensity enhancements in the line cores as those in the articles mentioned above.

In Fang et al. (2000) there were presented recalculated Hα line profiles, using higher relative precision, which exhibited lower intensity enhancements compared to those in Fang et al. (1993). Furthermore, according to Fang (private communication), a standard Lambda-iteration scheme was used as a method for solving the equation of radiative transfer in their papers (Fang et al. 1993; Hénoux et al. 1993). Due to these facts, we have also performed calculations by using the Lambda iterations. We have adopted the same values of parameters γ and Λ' as in Fang's paper ($\gamma = 15$, $\Lambda' = 9$). All line profiles presented in this section were convolved with a Gaussian macroturbulence velocity of 25 km s^{-1} in order to make a comparison with Fang's line profiles possible. Figure 6 shows Hα line profiles after 600 Lambda iterations for $\delta = 5$ and various values of $\mathcal{F}_1$. These line profiles are quite comparable to those in Fang et al. (1993, Fig. 1).

Moreover, Hα line source function after 600 Lambda iterations is also consistent with the one obtained in

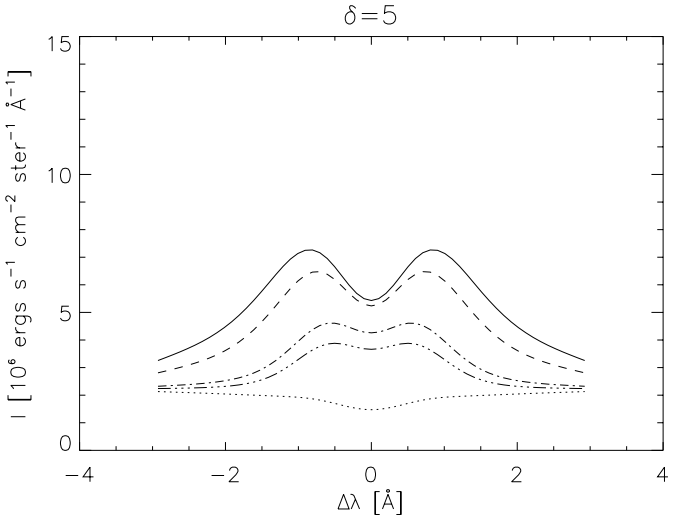

Fig. 6. Hα line profiles after 600 Lambda iterations for $\delta = 5$ and $\mathcal{F}_1 = 10^{12}$ (solid), 5×10^{11} (dashed), 10^{11} (dash dot), and $5{\times}10^{10}$ (dash dot dot dot) ergs cm^{-2} s^{-1}. Dotted line indicates the profile without including the non-thermal collisional rates. All profiles were convoluted with a Gaussian macroturbulence velocity of 25 km s^{-1}. For comparison see Fang et al. (1993, Fig. 1).

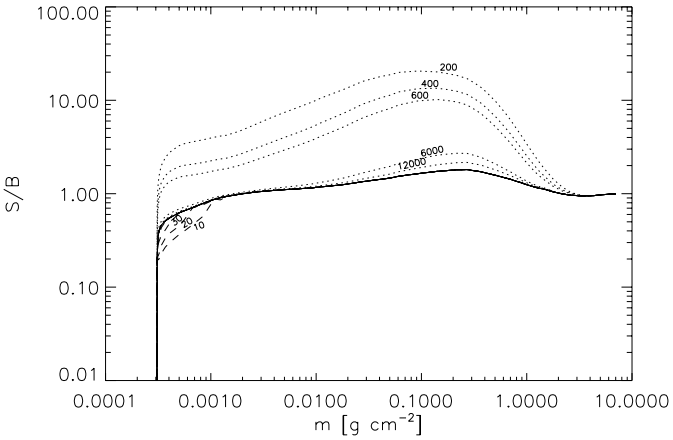

Fig. 7. Ratio of Hα source function S and Planck function B versus column mass m. The non-thermal collisional rates included with the beam parameters $\delta = 4$ and $\mathcal{F}_1 = 10^{12}$. MALI solution (solid), different numbers of Lambda iterations (dotted), and several MALI iterations (dashed).

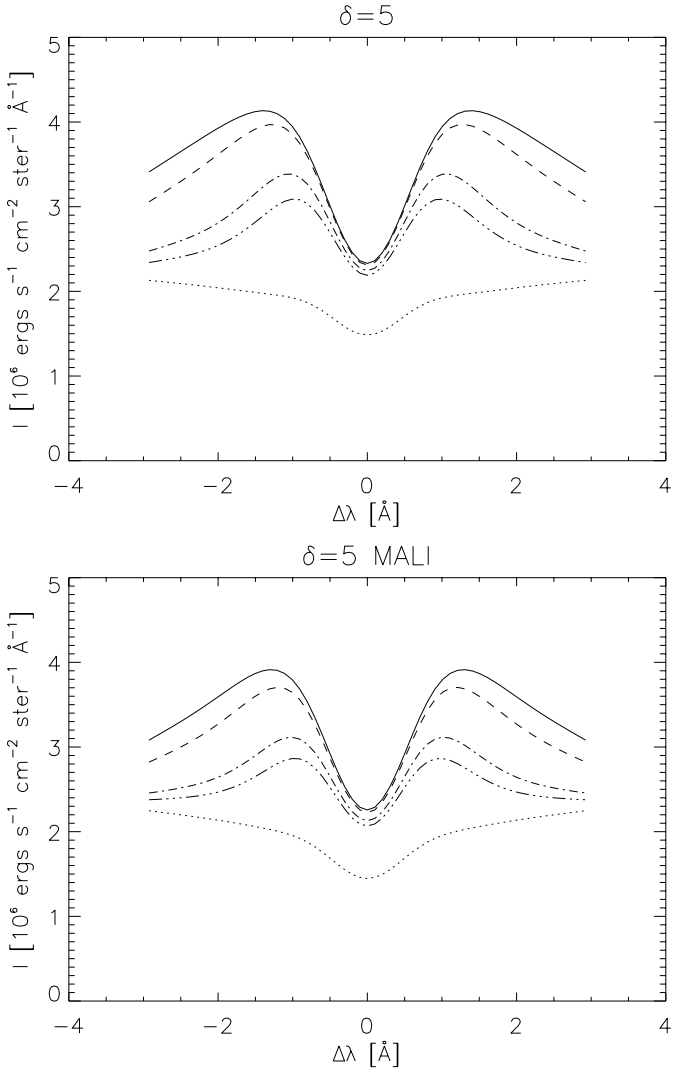

Fig. 8. Hα line profiles after 12 000 Lambda iterations (upper) and those computed by MALI method (lower) for $\delta = 5$ and $\mathcal{F}_1 = 10^{12}$ (solid), 5×10^{11} (dashed), 10^{11} (dash dot), and $5{\times}10^{10}$ (dash dot dot dot) ergs cm^{-2} s^{-1}. Dotted line indicates the profile without including the non-thermal collisional rates. All profiles were convoluted with a Gaussian macroturbulence velocity of 25 km s^{-1}.

Hénoux et al. (1993, Fig. 4). On the basis of these facts we can speculate that the slight difference between Fang's and our column mass dependence of the electron density for the model without including the non-thermal collisional rates is mainly due to the chosen numerical method. The electron density for the models with included non-thermal collisional rates is significantly affected by the non-thermal ionisation, which is the same in both Fang's and our calculations. Therefore, the influence of the chosen numerical method of the radiative transfer is suppressed and for the models with included non-thermal collisional rates our and Fang's electron densities are almost identical.

Figures 7 and 8 demonstrate behaviour of convergence of the standard Lambda-iteration method in the case of the flare atmosphere F1. Figure 8 shows that more than 12 000 standard Lambda iterations must be performed in order to obtain the Hα line profile comparable to that obtained by MALI method. Convergence of Hα source function for Lambda iterations and MALI iterations is displayed in Fig. 7. It is generally known that standard Lambda iterations converge very slowly at large optical depths (Mihalas 1978). The solution usually stabilises far from the true one after several tens or hundreds of iterations (Auer 1991; Heinzel 1995).

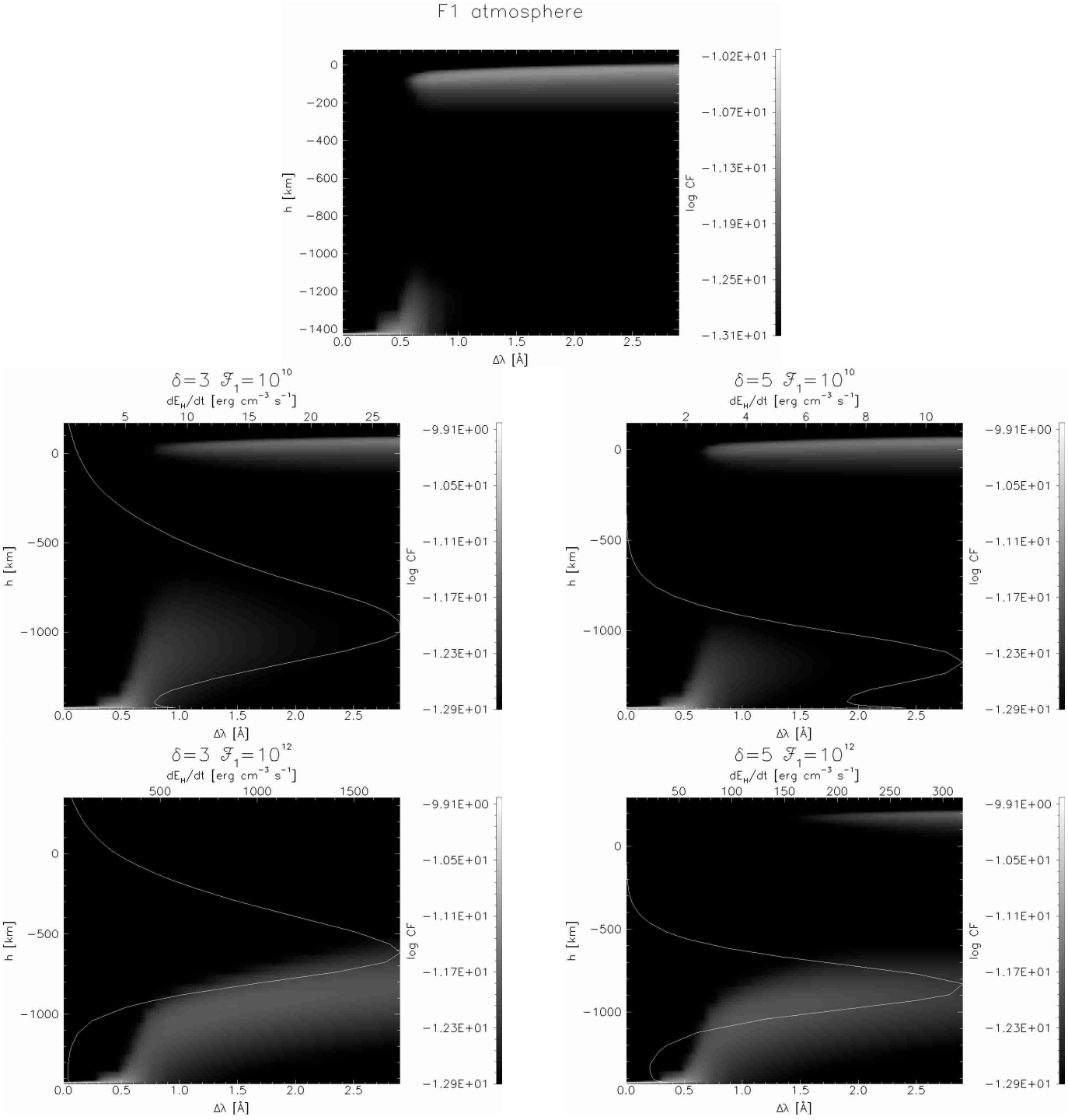

Fig. 9. Hα contribution function *CF* as a 2D function of the wavelength from the line centre and the depth h (positive values at the bottom of the atmosphere); grey scale represents values of *CF*. The first image shows *CF* without including the non-thermal collisional rates, the others correspond to *CF* for $\delta = 3$, 5 and $\mathcal{F}_1 = 10^{10}$, 10^{12} ergs cm^{-2} s^{-1}. The energy deposit rate on hydrogen d$E_{\rm H}$/dt is over-plotted on each of *CF* images with included non-thermal collisional rates.

6. Conclusions

In this paper we have studied an influence of the non-thermal collisional excitation and ionisation rates on the formation of first three hydrogen Balmer lines. Our results for the semi-empirical model F1 show that the line wings are sensitive to different values of beam parameters, mainly $\mathcal{F}_1$, whereas the intensity of line cores does not change significantly.

Moreover, the intensity ratios of Balmer lines appear to be considerably dependent on the total energy flux $\mathcal{F}_1$. We thus propose to use this effect as a diagnostic tool

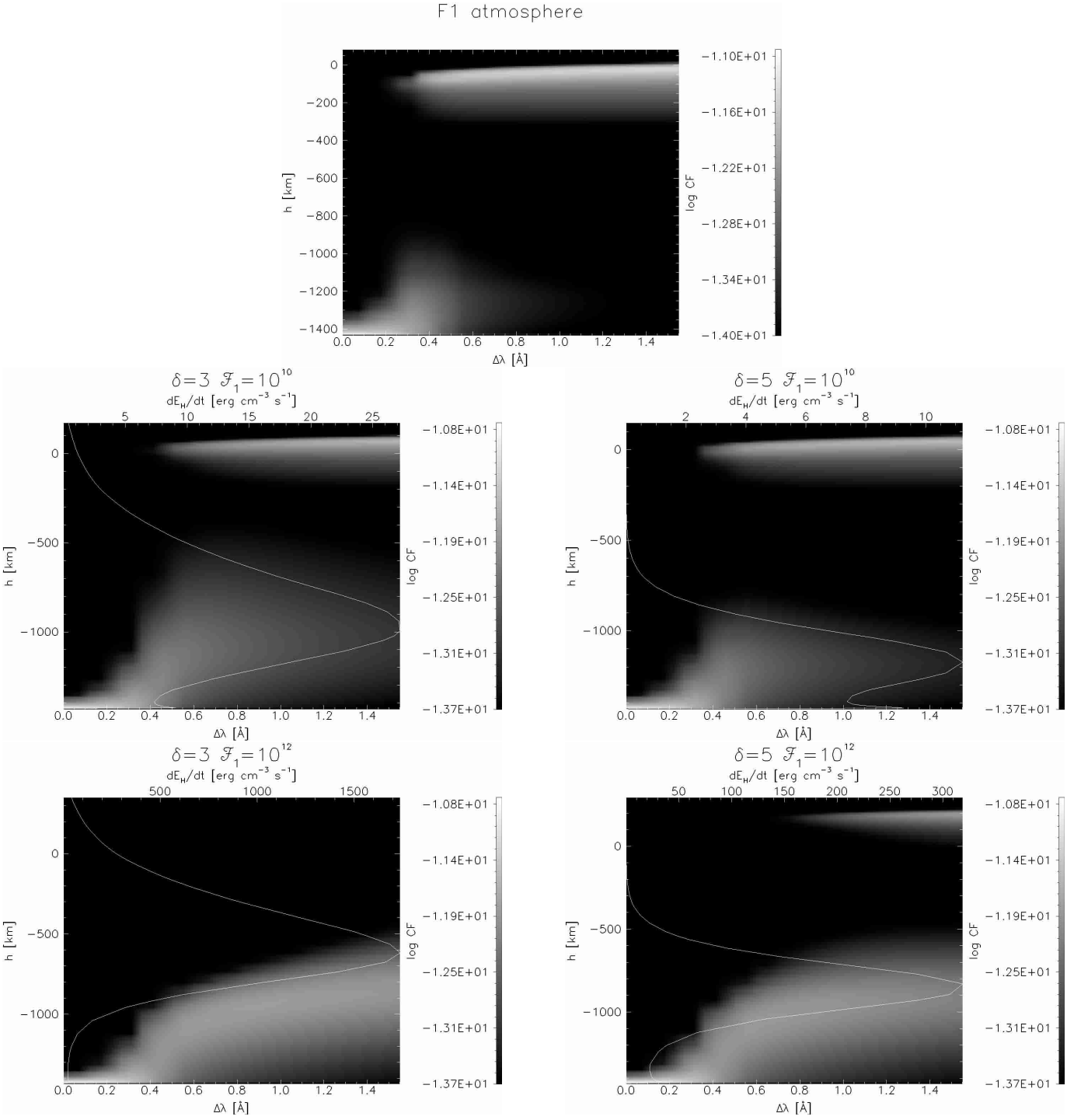

Fig. 10. Hβ contribution function *CF* as a 2D function of the wavelength from the line centre and the depth h (positive values at the bottom of the atmosphere); grey scale represents values of *CF*. The first image shows *CF* without including the non-thermal collisional rates, the others correspond to *CF* for $\delta = 3$, 5 and $\mathcal{F}_1 = 10^{10}$, 10^{12} ergs cm^{-2} s^{-1}. The energy deposit rate on hydrogen d$E_{\rm H}$/dt is over-plotted on each of *CF* images with included non-thermal collisional rates.

for revealing the presence of electron beams during impulsive phases of solar flares. However, one must bear in mind that the relations presented here do not include possible changes of the temperature structure during the flare evolution.

In our case we have treated the atmosphere in a semi-empirical manner keeping same temperature distribution of model F1 for all our models. The model F1 was derived on base of flare spectra (mainly the UV continua) and does not include the non-thermal collisional rates. Therefore, in

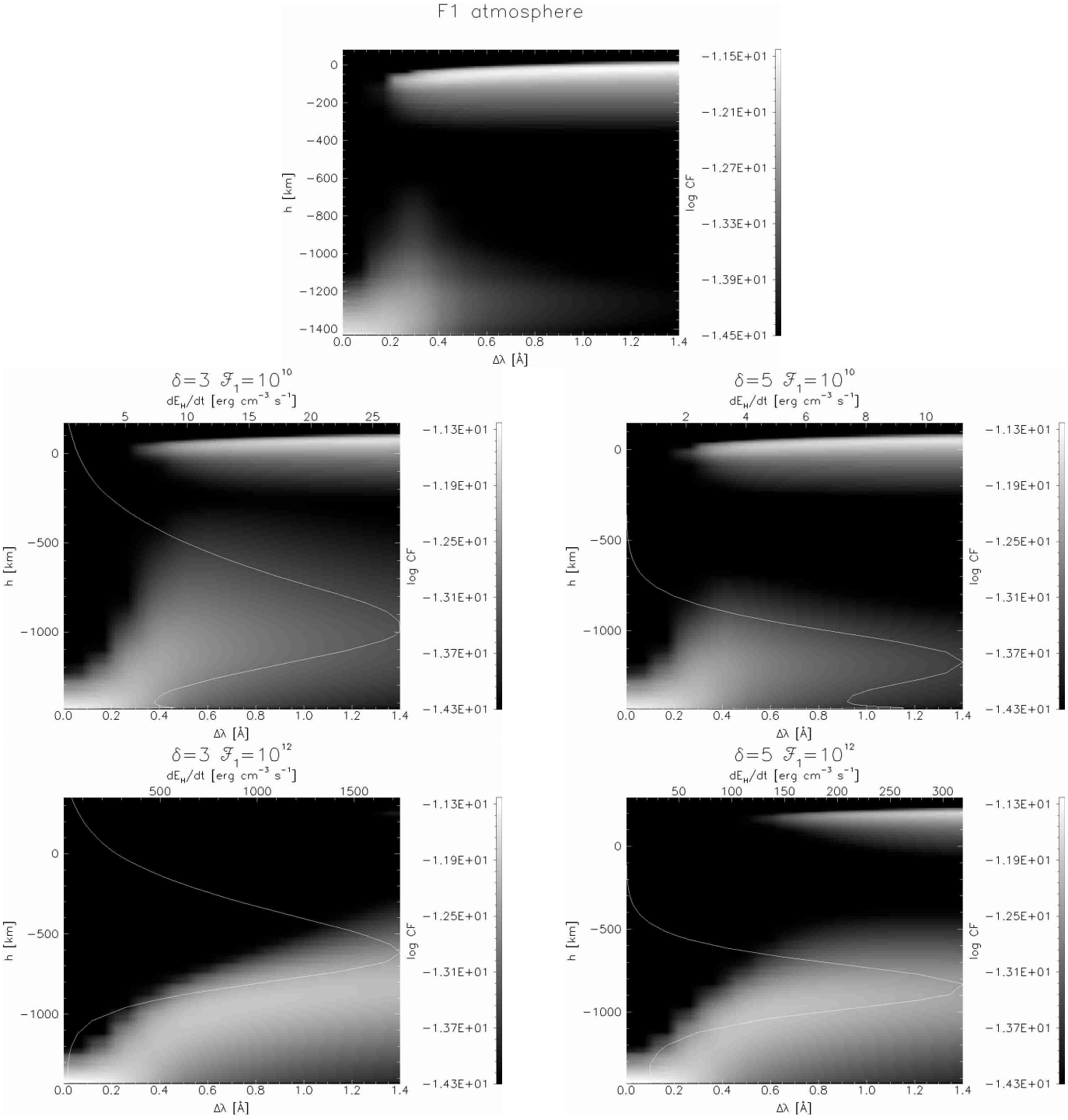

Fig. 11. Hγ contribution function *CF* as a 2D function of the wavelength from the line centre and the depth h (positive values at the bottom of the atmosphere); grey scale represents values of *CF*. The first image shows *CF* without including the non-thermal collisional rates, the others correspond to *CF* for $\delta = 3$, 5 and $\mathcal{F}_1 = 10^{10}$, 10^{12} ergs cm^{-2} s^{-1}. The energy deposit rate on hydrogen d$E_{\rm H}$/dt is over-plotted on each of *CF* images with included non-thermal collisional rates.

the presence of the beam, the F1 temperatures, which we use, are actually overestimated (the non-thermal excitations produce a part of the line and continuum emission). In this sense, our present simulations are only aimed at analysing the differential effects as discussed above.

Furthermore, we have assumed that beam of electrons penetrates through the atmosphere which is in hydrostatic equilibrium (model F1). This simplification is valid only when motions are negligible in the flare atmosphere. However, the equilibrium solution with the non-thermal collisional rates results in a change of electron density that modifies number density of hydrogen which subsequently changes the geometric depth scale. This leads to a new density distibution on h compared

to the model F1. In reality, the presence of the beam will cause a dynamical evolution of an atmosphere.

Finally, using a five-level plus continuum model of hydrogen atom may not be sufficient in the case of Hγ line. An atomic model with more levels included should be considered to obtain quantitatively more accurate results which could be compared with the observations.

This analysis gives us an insight into the non-thermal effects introduced by electron beams which will be used in our future work. We plan to develop time-dependent models of the beam heating by a series of short duration pulses of accelerated beams of electrons and/or protons.

Acknowledgements. This work was partially supported by the grant A3003902 of the Academy of Sciences of the Czech Republic. The authors are indebted to J.-C. Hénoux for useful discussions and comments.

References

Auer, L. 1991, in NATO ASI Series C 341, Stellar Atmospheres: Beyond Classical Models, ed. L. Crivellari, I. Hubeny, & D. G. Hummer (Kluwer Academic Publisher), 9
Brown, J. C. 1972, Solar Phys., 29, 421
Canfield, R. C., Gunkler, T. A., & Ricchazzi, P. J. 1984, A&A, 282, 296
Chambe, G., & Hénoux, J.-C. 1979, A&A, 80, 123
Emslie, A. G. 1978, ApJ, 224, 241
Emslie, A. G. 1981, ApJ, 245, 711
Fang, C., Ding, M. D., Hénoux, J.-C., & Gan, W. Q. 2000, in Proceedings of the First Franco-Chinese Meeting on Solar Physics, ed. C. Fang, J.-C. Hénoux, & M. D. Ding, 147
Fang, C., Hénoux, J.-C., & Gan, W. Q. 1993, A&A, 274, 917
Hawley, S. L., & Fisher, G. H. 1994, ApJ, 426, 387
Heinzel, P. 1995, A&A, 299, 563
Hénoux, J.-C. 2000, in Anticipating HESSI, ed. R. Ramaty, & N. Mandzhavidze, ASP Conf. Ser., 206, 27
Hénoux, J.-C., Fang, C., & Gan, W. Q. 1993, A&A, 274, 923
Hudson, H. S. 1971, Solar Phys., 24, 414
Lin, R. P., & Hudson, H. S. 1976, Solar Phys., 50, 153
Machado, M. E., Avrett, E. H., Vernazza, J. E., & Noyes, R. W. 1980, A&A, 242, 336
Mihalas, D. 1978, Stellar Atmospheres (W. H. Freeman and Company), 148
Ricchiazzi, P. J. 1982, Ph.D. Thesis, University of California
Ricchiazzi, P. J., & Canfield, R. C. 1983, ApJ, 282, 739
Rybicki, G. B., & Hummer, D. 1991, A&A, 245, 171